Effect of sintering temperatures on the mechanical properties of the ceramics was studied by Vickers and Knoop microhardness testers. Indentations were applied on the polished surfaces of PZ ceramics. Applied loads were in the range of 200–1000 g with an indentation period of 15 s. Indentation crack length (c) and indentation diagonal (d) was measured, and then used to calculate Vickers hardness, Knoop hardness and fracture toughness by the following equations:

$$H_V = 1854.4 \left(\frac{P}{d_v^2}\right) \tag{1}$$

where H_V is a Vickers hardness (in GPa), d_V (in μ m) and P is an applied load (in N).

$$H_K = 1.451 \left(\frac{P}{d_K^2}\right) \tag{2}$$

where H_K is a Knoop hardness (in kg/mm²), d_K is a longer diagonal length of a Knoop indentation (in mm) and P is an applied load (in N).

$$K_{IC} = \xi \left(\frac{E}{H_V}\right)^{1/2} \left(\frac{P}{c^{3/2}}\right) \tag{3}$$

where K_{IC} is a fracture toughness (in MPa·m^{1/2}), H_V is a Vickers hardness (in GPa), P is an applied load (in N), E is Young's modulus (in GPa) and c is the radial length measured from the centre of indentation impression (in m) [10, 11], ξ is a material independent, dimensionless calibration constant which characterizes the geometry of the deformation filed. Studies on many ceramics led to an average value of $\xi = 0.016 \pm 0.004$ [12]. After indentation, the samples were etched by 10% HCl + 1 drop HF. Microstructure of the etched samples was again studied by SEM.

RESULTS AND DISCUSSION

Effect of calcination temperatures on the phase formation of the PZ powder was shown by XRD patterns in Fig. 1. At the calcination temperatures starting from 775°C, a single phase of PZ was detected. The phase analysis was carried out based on the Joint Committee on Powder Diffraction Standard (JCPDS) [1]. The density and Curie temperature of PZ ceramics were plotted as a function of sintering temperature are shown in Fig. 2. The value of density is in the range of 7.88–7.95 g/cm³ or 97.68–98.48% of the PZ theoretical

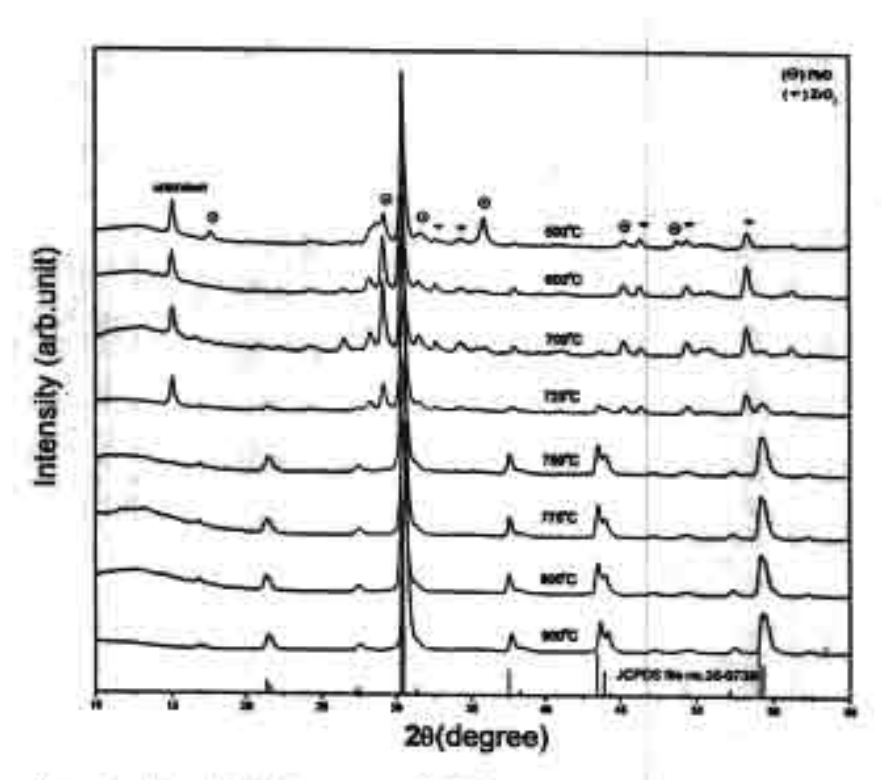


Figure 1. X-ray diffraction patterns of PbZrO3 calcined at different temperatures.

density. The density increases with increasing the sintering temperature up to 1200°C and decreases with further increasing the sintering temperature. The maximum value of density is 98.48% of the theoretical density, observed in the ceramic sintered at 1200°C. Decreasing of the density is likely due to a vaporization of PbO at the temperatures above 1200°C [14]. Figure 3 shows the plot of grain size and porosity as a function of sintering temperature. Grain size of the samples is in the range of 0.9 to 1.5 μ m and found to slightly increase with the increasing of the sintering temperature. Weight loss of the PZ ceramics as a function of sintering temperature is shown in Fig. 4. The weight loss increased with increasing the sintering temperature as expected.

The temperature dependences of dielectric constant and dissipation factor at various sintering temperatures were studied and as shown in Table I and plotted in Fig. 5. The measurement of dielectric constant at room temperature is in the range of 157 to 170, while the dissipation factor ($\tan \delta$) is in the range of 0.0042 to 0.0205. The highest dielectric constant at room

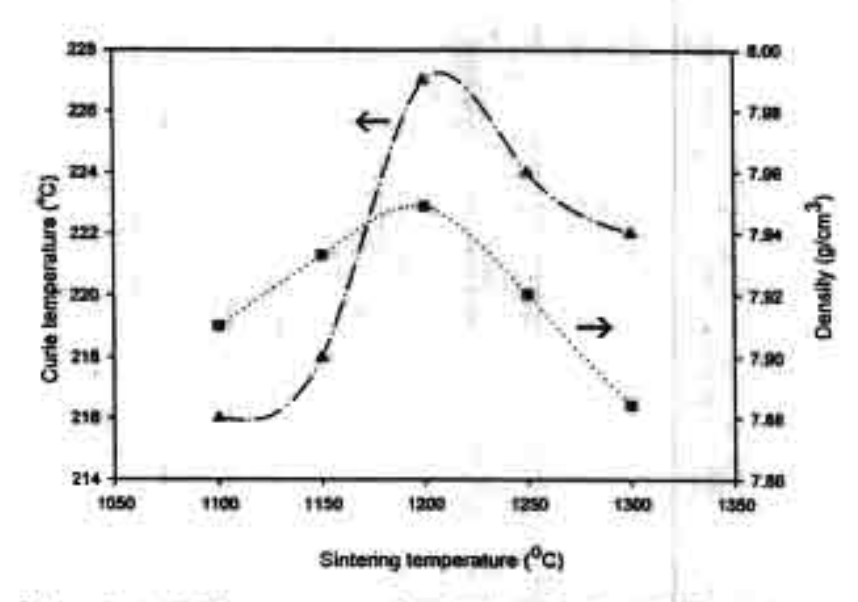


Figure 2. (A) Curie temperature and (III) density of the samered PZ ceramics with sintering temperature.

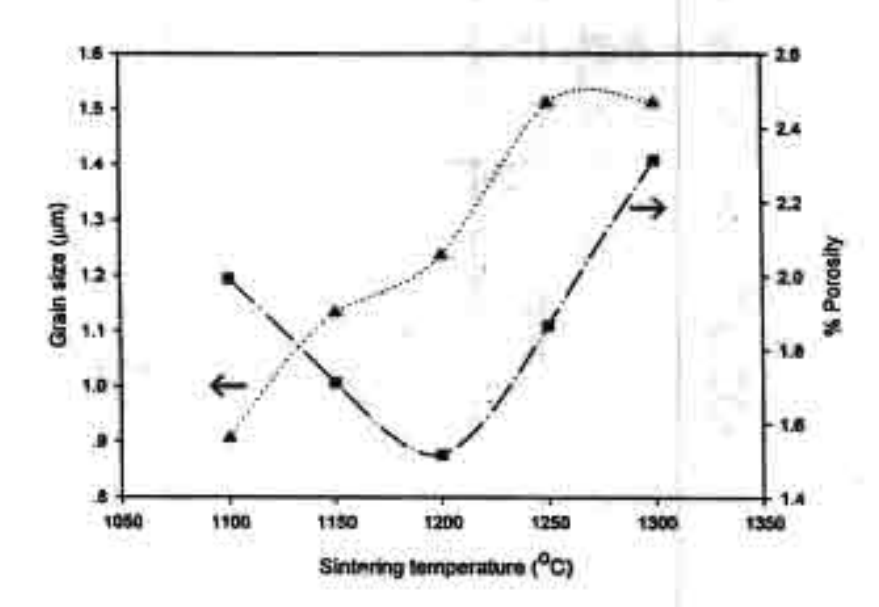


Figure 3. (A) Grain size and (III) porosity as a function of sintering temperature.

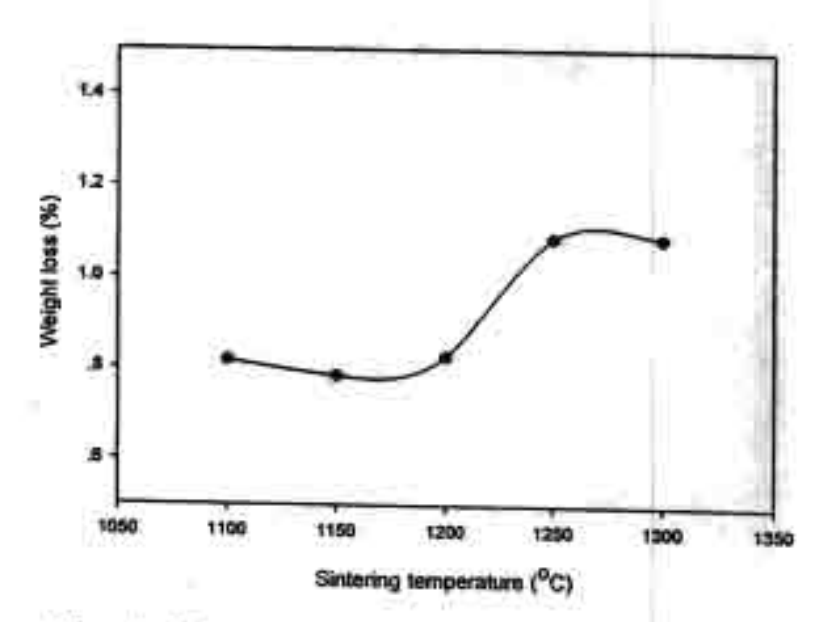


Figure 4. Weight loss of PZ ceramics at various sintering temperatures.

temperature is 170, observed in the PZ ceramic sintered at 1200°C with the grain size of 1 μ m. Kong et al. prepared PZ ceramics from high-energy ball-milling method and found that the dielectric constant of their PZ ceramic decreases at the higher sintering which is caused by the loss of PbO [13]. The highest dielectric constant in their work is about 218 for the sample sintered at 1200°C with grain size of 8 μ m. However, the highest value of the dielectric constant ($\epsilon_r = 170$) at room temperature in our work for the ceramics with 1 μ m grain size is close to the value found in their work.

TABLE I Dielectric properties of PbZrO₃ ceramics sintered at different temperatures

Sintering temperature (°C)	Dielectric constant at 27°C	Dissipation factor at 27°C	Curie temperature (°C)
1100	163	0.0042	227
1150	157	0.0147	228
1200	170	0.0205	232
1250	155	0.0230	231
1300	164	0.0229	230

The variation of Curie temperature as a function of the sintering temperature is also shown in Fig. 5. The maximum dielectric constants at the phase transition temperature are between 6750 and 7762, while Robert [9] and Shirane [5] reported the maximum values of dielectric constant at the phase

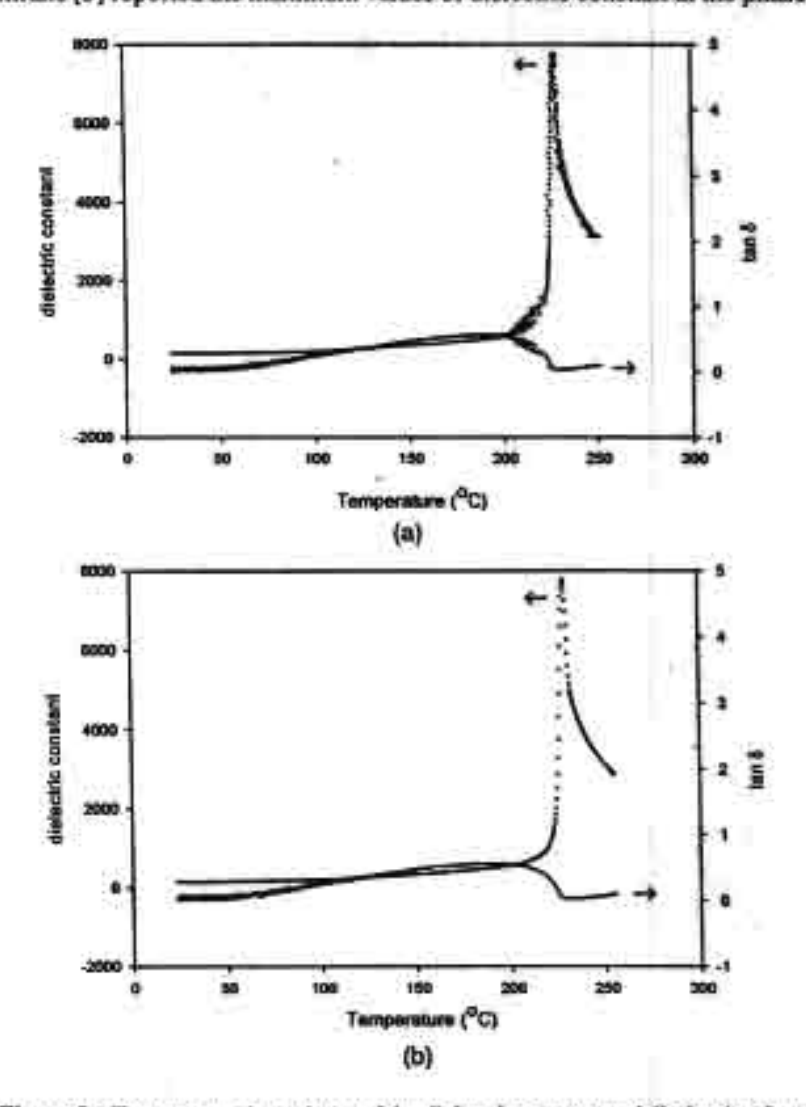


Figure 5. Temperature dependence of the dielectric constant and dissipation factor of PZ sintered at: (a) 1100°C, (b) 1150°C, (c) 1200°C, (d) 1250°C, and (e) 1300°C, (Continued)

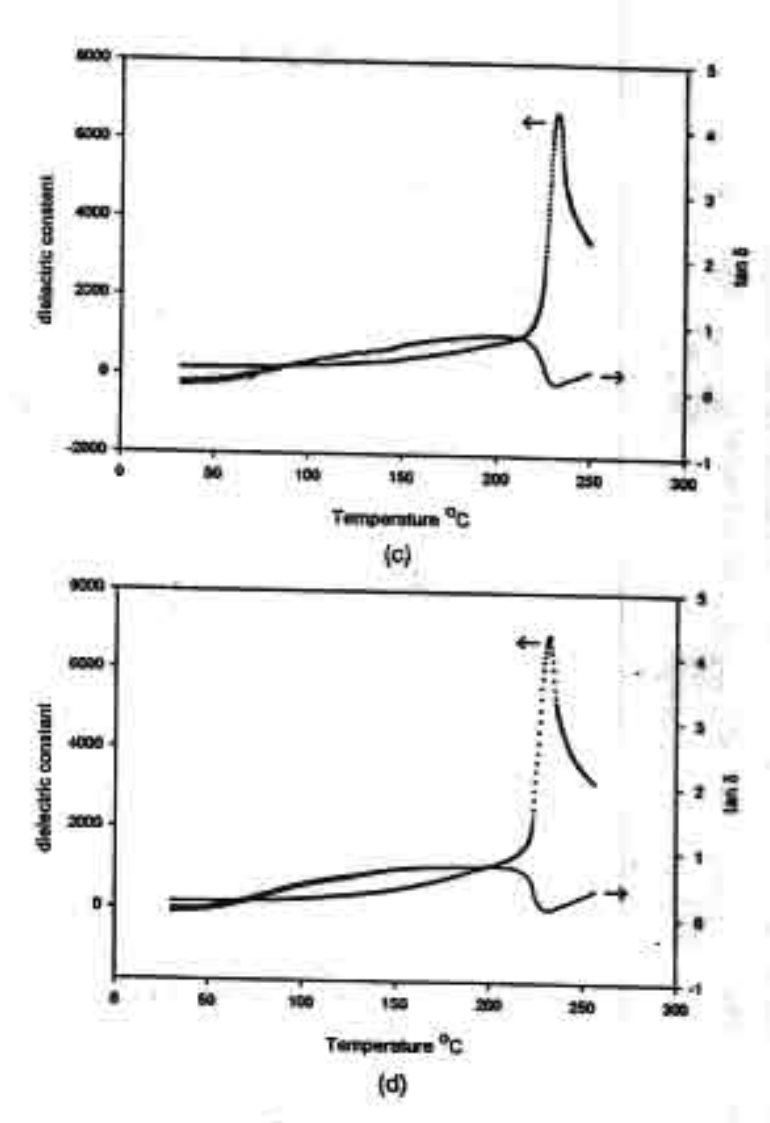


Figure 5. (Continued)

transition temperature are approximately 3260 and 2300, respectively. In the present work, the Curie temperature increases with the sintering temperature up to 1200°C and then decreases with further increasing the temperature. It can be noted that the Curie temperature results are well corresponded to the density results. This is well corresponded with the work done on a

Figure 5. (Continued)

ferroelectric materials, i.e., BaTiO₃ by Fang et al., where the Curie temperature increased with increasing the density of BaTiO₃ which is a ferroelectric materials [14].

The effect of sintering temperature on the mechanical properties of the samples was studied by using Vickers and Knoop microhardness testers. The values of Vickers hardness, Knoop hardness, and fracture toughness are listed in Table II, and the plot of these values as a function of sintering temperature are shown in Fig. 6. The hardness values trend to decrease as increasing the sintering temperatures. This result would be well corresponding

TABLE II Mechanical properties of PbZrO₃ ceramics sintered at different temperatures

Sintering temperature (*C)	Victors hardness (GPa)	Knoop hardness (GPa)	Fracture toughness (MPa-m ^{1/2})
1100	5.37	4.42	1.38
1150	4.85	4.54	2.91
1200	4.77	4.49	2.91
1250	4.50	4.46	1.97
1300	4.65	3.94	1.12

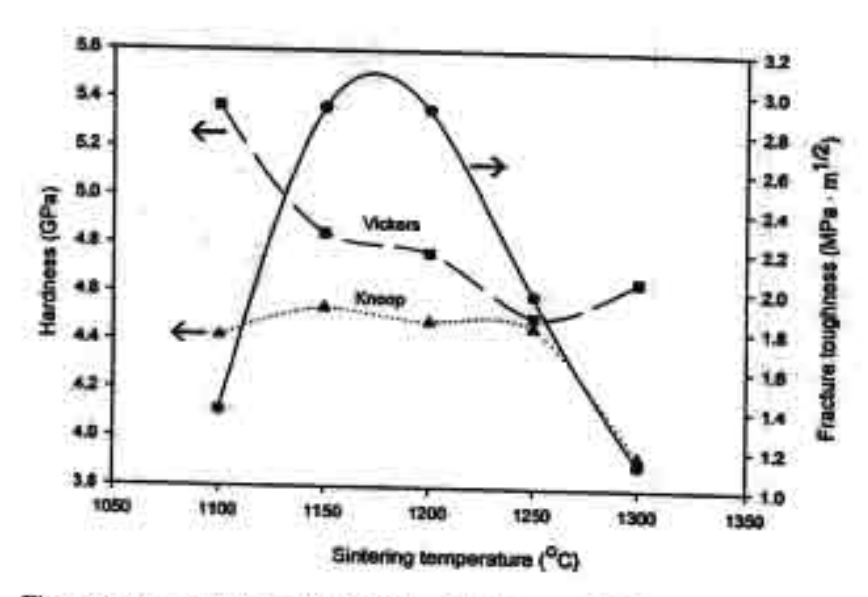


Figure 6. (A.B) Hardness and (a) fracture toughness of the PZ cerumics plotted as a function of sintering temperatures.

with the density (Fig. 2.) and porosity (Fig. 3.) results, where they are significantly changed due to the loss of PbO at the temperature above 1200°C. For the fracture toughness values which were calculated mainly from the hardness and crack extension from the Vickers indentation impressions, seem to depend significantly on the density and porosity as well. The fracture toughness dramatically increases with the sintering temperature up to I 150°C and then decreases with further increasing the temperature. Figure 7(a) and (b) are SEM micrographs of Vickers and Knoop indentations performed on polished PZ samples sintered at 1200°C. The examples of crack characteristic extended from the Vickers indentation impressions are shown in Fig. 7(c) and 7(d). The cracks of PZ sintered at 1150°C are followed the grain boundaries, so called intergranular crack (Fig. 7(c)), while those cracks found in the sample sintered at 1300°C are rather straight through the grains indicating transgranular fracture (Fig. 7(d)). According to the Table II, the fracture toughness value of PZ sintered at 1150°C ($K_{IC} = 2.91 \text{ MPa} \cdot \text{m}^{1/2}$) is higher than that of PZ sintered at 1300°C ($K_{IC} = 1.12 \text{ MPa-m}^{1/2}$). This result is well corresponding to the microstructure; the higher the fracture toughness, the harder the crack cut through the grains and vice versa. Generally, the

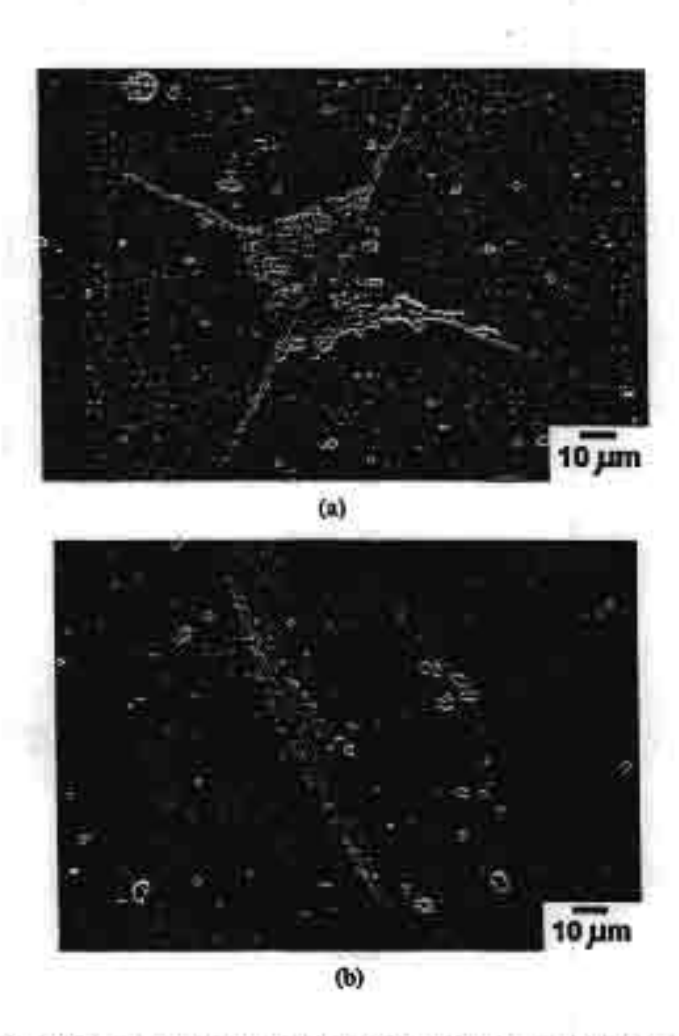


Figure 7. SEM micrographs of (a) Vickers indentation on surface of PZ sintered at 1200°C, (b) Knoop indentation on surface of PZ sintered at 1200°C, (c) indentation crack of PZ sintered at 1300°C, and (d) indentation crack of PZ sintered at 1300°C. (Continued)

hardness and fracture toughness of lead base ceramics depends on many factors such as grain size and porosity [15, 16]. In the present work, the reduction of hardness and fracture toughness at higher sintering temperature is likely to cause by the loss of PbO during sintering which form the lower density and imperfect ceramics [13].

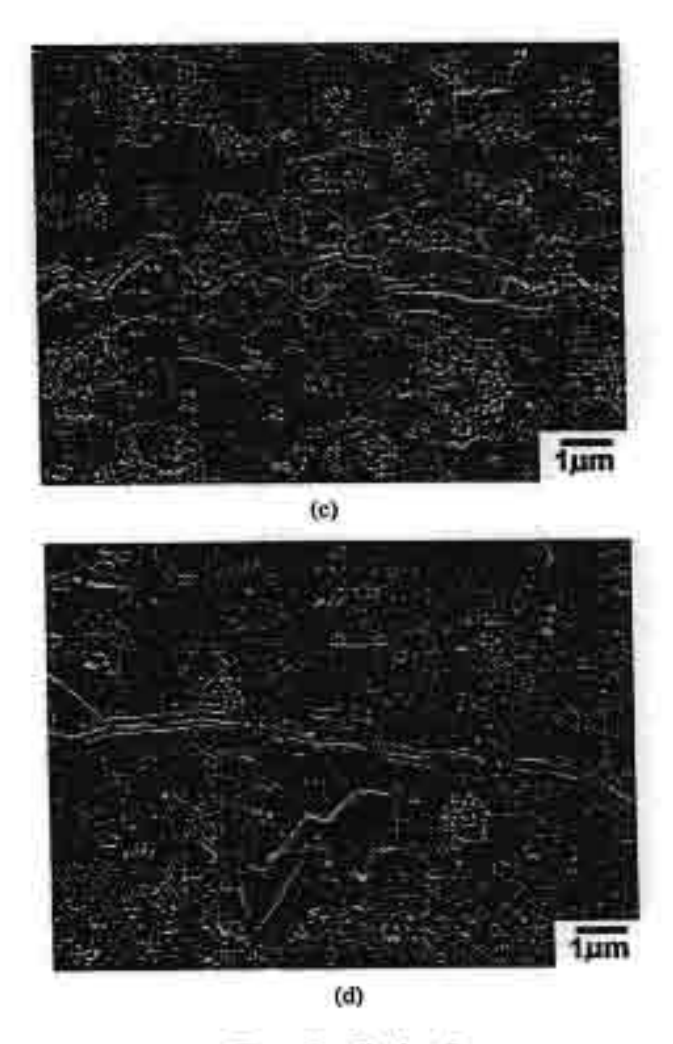


Figure 7. (Continued)

CONCLUSIONS

In the present work, the PbZrO₃ (PZ) was prepared via the mixed oxide method. The single phase of PZ was found in the powders calcined at the temperature ≥775°C. The sintering temperature has effects on phase transition behavior and mechanical properties of the PZ. Carie temperature and density of the PZ ceramics increased with increasing sintering temperature

up to 1200°C. However, they decreased for higher sintering temperature. The lower density is likely to cause by the loss of PbO during sintering above 1200°C which then result to the reduction of density, Curie temperature, hardness, and fracture toughness values.

ACKNOWLEDGMENTS

We would like to thank the Thailand Research Fund, Graduate School, Chiang Mai University, Faculty of Science Chiang Mai University, and Ministry of University Affairs for financial support throughout the project.

REFERENCES

- Powder Diffraction File, Card No. 35-0739. Joint Committee on Powder Diffraction Standards (JCPDS) PDF-4. Internation Centre for Diffraction Data (JCDD), 2000.
- [2] B. Jaffe, W. R. Cook, and H. Jaffe, Piezoelectric cerumics (R.A.N. Publishers, 1971), pp. 123-131.
- [3] E. E. Oren, E. Taspinar, and A. C. Tas, J. Am. Cerum. Soc. 80(10), 2714 (1997).
- [4] M. T. Lanagan, J. H. Kim, S. Jang, and R. E. Newnham, J. Am. Ceram. Soc. 71(4), 311 (1988).
- [5] G. Shirane, Phys. Rev. 86(2), 219 (1952).
- [6] B. P. Pokharel, M. K. Datta, and D. Pandey, J. Mater. Sci. 34, 691 (1999).
- [7] B. P. Pokharel and D. Pandey, J. Appl. Phys. 88(9), 5364 (2000).
- [8] K. H. Yoon, S. C. Hwang, and D. H. Kang, J. Mater. Sci. 32, 17 (1997).
- [9] S. Roberts, J. Am. Ceram. Soc. 33(2), 63 (1950).
- [10] D. B. Marshall and B. R. Laws, J. Mar. Sci. 14, 2001 (1979).
- [11] B. R. Lawn, A. G. Evuns, and D. B. Marshall, J. Am. Ceram. Soc. 63, 574 (1980).
- [12] G. R. Anstis, P. Chuntikul, B. R. Lawn, and D. B. Marshall, J. Am. Cerom. Soc. 64(9), 533 (1981).
- [13] L. B. Kong, J. Ma, W. Zhu, and O. K. Tan, Morer. Lett. 49, 96 (2001).
- [14] T. Fang, H. Hsieh, and F. Shinu, J. Am. Cerom. Soc. 76(5), 1205 (1993).
- [15] K. Uchino, Piezoelectric Actuarors and Ultrasonic Motors (Klawer Academic Publishers, 1997), pp. 113–114.
- [16] D. R. Biswas and R. M. Fufruth, Trans. J. Brit. Cer. Soc. 79, 1 (1980).

Manuscript ผลงานวิจัยที่อยู่ในขั้นตอนการตอบรับและดี พิมพ์ในวารสารวิชาการระดับนานาชาติ lanuscript for submission to Materials Lette

Effect of excess PbO on phase formation and properties of (Pb0,90Ba0,10) ZrO3 ceramics

Theerachai Bongkarn, Gobwute Rujijanagul*

Department of Physics, Faculty of Science, Chiang Mai University, 50200 Thailand

Steven J Milne

Institute for Materials Research, University of Leeds, Leeds, LS2 9JT, UK.

Abstract

Polycrystalline samples of Pb0.9Ba0.1ZrO3 (PBZ) were prepared by a mixed oxide, solid-state

reaction method. Excess PbO (3, 5 or 10 wt %) was introduced prior to powder calcination to

compensate for any PbO that may have been lost from the samples due to volatilisation during

heat treatments. X-ray diffraction revealed that, compared to samples made from

stoichiometric starting mixtures, a starting excess of PbO of ≥ 3 wt % increased the

proportion of the rhombohedral PBZ phase which coexisted with the antiferroelectric

orthorhombic phase. Microstructurally, excess PbO produced an increase in average grain

size, from ~ 1 µm for no excess to ~1.5 µm for ≥ 3 wt % excess PbO. The fractured surfaces

indicated predominantly intra-granular fracture in samples with no added PbO, or 3 wt %

excess PbO, whereas the 5 and 10 wt % excess PbO samples displayed mainly inter-granular

fracture. Dielectric constant-temperature plots showed a maximum peak value of 12700, for

the 3 wt % sample which was also the most dense sample.

Keywords: lead barium zirconate; phase stability; excess lead oxide.

*Corresponding author. Tel.: +66-53-943-376; fax: +66-53-357-512

E-mail address: rujijanagul@yahoo.com (Gobwute Rujijanagul)

1. Introduction

Lead zirconate, PbZrO₃, is a well-known antiferroelectric possessing an orthorhombic structure in which the origin of antiferroelectricity is an antiparallel shift of Pb ions along the [110] direction [1-4]. The transition to the paraelectric phase occurs at around 235 °C but a transition from the orthorhombic antiferroelectric (AFE) structure to a rhombohedral ferroelectric (FE) structure a few degrees below the paraelectric transition temperature has been reported by several authors [5, 6]. Weak ferroelectric properties have also been reported at room temperature, and it has been proposed that PbZrO₃ exhibits competing ferroelectric and antiferroelectric modes [4]. The temperature range over which the FE phase is stable can be extended by application of an electric field or by chemical substitution, such as Ba ²⁺ on the Pb ²⁺ sites to form (Pb_{1-x}Ba_x)ZrO₃ solid solutions [7-15]. The AFE-FE phase transition produces an ~ 1 % increase in volume for polycrystalline (Pba₂Ba_{0.10})ZrO₃ (PBZ) [15], and the electric-field required to induce AFE-FE switching is much lower than for PbZrO₃ (PZ) which has created interest in PBZ for potential use in large displacement actuator devices requiring low switching voltages [13].

Shirane [7] was one of the first to demonstrate the AFE \rightarrow FE phase transition in $(Pb_xBa_{1-x})ZrO_3$ solid solution compositions with $x \ge 0.05$. However several other authors [10-11] have found no evidence of any AFE-FE transitions, whilst some report [13] an AFE \rightarrow FE transition but no corresponding FE \rightarrow AFE transition on cooling. It has been proposed that the occurrence of a AFE \rightarrow FE transition on heating, but no reverse cooling transition, is because the transformation is subject to a large temperature hysteresis, shifting the FE phase transition to below room temperature on the cooling cycle [14]. An alternative explanation is that the FE \rightarrow AFE phase transition is sluggish and the FE phase is quenched to

room temperature [13]. It has also been reported that the AFE phase can reappear after longterm (several months) aging [13].

The processing method used to prepare the PBZ powders may also be important in influencing phase formation and in explaining why different research groups report different results. It has been suggested that the AFE→FE transitions are sensitive to the chemical homogeneity of the Ba and Pb ions [14], and, as is the case for PZ, to chemical impurities. The rhombohedral FE phase is more likely to be observed using powder processing routes which promote homogeneous distributions of Ba and Pb ions and/or low levels of impurities which promote homogeneous distributions of Ba and Pb ions and/or low levels of impurities [6]. Small quantities of certain impurities, particularly Ca (0.05 wt%), are sufficient to completely supress the FE rhombohedral phase [6]. However another factor to consider is the possible effect of PbO loss due to evaporation during high temperature processing [14]. Any variation in Pb and O ion vacancy concentrations may be important in terms of phase stability. Despite efforts to suppress PbO loss by using PZ 'atmosphere' powders to generate a PbO vapour above the sample during sintering, PbO losses may still arise, particularly as powder calcination, prior to sintering, is usually carried out in open-crucibles to facilitate barium carbonate decomposition at 700-850°C [12]. Even at these moderate temperatures, the PbO vapour-pressure may be sufficient to create compositional changes in the powders.

To our knowledge, the effect of influencing PbO stoichiometry in PBZ, through additions of a compensating excess of PbO to the starting powders has not been reported. However additions of excess PbO are often carried out in the processing of other Pb-based ceramics as a means of improving electrical properties, and also for improving densification by promoting a liquid phase during sintering [16-26].

In this communication, we report for the first time our results showing a dependence of PBZ phase stability on the PbO content of the starting powders. Results are also reported for microstructure, densification, and dielectric properties.

2. Experimental procedure

The (Pb_{0.9}Ba_{0.10})ZrO₃ powders were prepared by a conventional mixed oxide route employing PbO (purity 99.9%, supplied by Johnson Matthey GmbH, UK), ZrO₂ (purity 99%, supplied by Aldrich, UK) and BaCO₃ (purity 99.9%, supplied by Johnson Matthey GmbH, UK). The powders were weighed and mixed by ball milling for 24 h in acetone using zirconia grinding media. After drying and sciving, the mixture was calcined at 850 °C for 6 h. An excess of PbO, equivalent to 3, 5 or 10 wt% was added prior to ball milling. The calcined powders were reground by ball-milling with 1 wt% binder (B-5 supplied by Rohn-Haas, Germany) for 24 h. The powders were then dried, crushed and sieved again. Pellets 15 mm in diameter were isostatically pressed at 80 MPa. Finally, the pellets were sintered at 1325°C for 4 h.

In order to help control PbO loss during sintering (in addition to adding excess PbO) a PZ 'atmosphere'powder was used to generate PbO vapour over the samples. The microstructures of the sintered samples were examined using scanning electron microscopy (JEOL, JSM6335F). Phase formation in the calcined powders and the sintered pellets was determined using an X-ray powder diffractometer (Phillips ADP1700). The density of the sintered samples was measured by Archimedes' method with distilled water as the fluid medium. The dielectric measurements were carried out at 1 kHz using a HIOKI 3532-50 impedance analyzer, from room temperature to 270°C, at a heating rate of 0.5°C/min.

3. Results and discussions

Fig. 1 show XRD patterns of calcined powders made from starting mixtures containing different levels of PbO. For the sample made with no excess PbO, only the PBZ phase was observed [12]. On the other hand, small amounts of PbO [28-29] and PbZrO₃ [27] were clearly present in the 10 wt % excess PbO sample, and there was also some evidence of these phases being present, in the 5 wt %, and to a much lesser extent, in the 3 wt % samples. Although the presence of 'free' PbO is expected in the higher excess samples, the results indicate that additions of PbO produce a three-phase mixture including PbZrO₃.

Pockarel and co-workers [12, 13] have reported on the phase stability in Pb1-xBaxZrO3 powders as a function of both Ba content, and the method of preparing the powders. Based on crystallographic data available for PZ, they qualitatively demonstrated changes in the amounts of AFE orthorhombic and FE rhombohedral phases in PBZ, based on variations in measured XRD peak intensities. The d-spacings of the main peaks are similar for rhombohedral and oththorhombic PBZ patterns, however certain weak relections are present in the XRD patterns of the orthorhombic phase but not in the rhombohedral phase, for example the 130/112, 210 and 230/212 reflections [13]. In addition, due to peak overlap effects between rhombohedral and orthorhombic structures, the intensity of the peak indexed as 240 in the orthorhombic pattern (200 in the rhombohedral structure) is increased relative to the neighbouring 004 peak by the presence of the rhombohedral phase [13]. The intensity ratio of 004/240 peaks may therefore be taken as a qualitative indicator of the relative proportions of orthorhombic (AFE) and rhombohedral (FE) phases. For a purely orthorhombic pattern, I 004/240 ~ 0.5, and this value decreases with increasing amounts of co-existing rhombohedral phase [13]. The relative intensities of 120/002 and 322/044 peaks also change in a similar manner with increasing proportions of rhombohedral phase.

The relative intensity of XRD peaks distinctive of the orthorhombic phase, are plotted as a function of PbO content in Fig. 2a It is apparent that on adding 3 wt % excess PbO there was a significant decrease in the intensity of orthorhombic reflections in the calcined powders. Higher excesses produced little further change in intensities. There was also a decrease in the value of the intensity ratio I_{004/240}, from a value of 0.47 for 0 % starting excess PbO to values of ~ 0.15-0.2 for the 3- 10 wt % PbO samples, Fig. 2b These results indicate that the introduction of excess PbO increases the proportion of rhombohedral phase in PBZ calcined powders. The structural reasons for this are uncertain at this stage, but the result may indicate that Pb and O ion vacancies in uncompensated compositions de-stabilise the rhombohedral (FE) structure.

The XRD data for sintered samples revealed that no PbO (or PZ) was present in any sample, indicating that the excess PbO beyond that required to maintain compositional control (assumed) in the PBZ powder was eliminated from the sample by volatilisation during sintering at 1325 °C. The corresponding intensity ratio I 1004/240 is plotted in Fig. 2b. Although the trend was similar to that of the calcined powders, the intensity ratio for all sintered samples was higher, suggesting less rhombohedral and more orthorhombic phase in the sintered pellets. Based on the interpretation of the XRD results for calcined powders, this would be consistent with a lower PbO content in the sintered PBZ crystal structure than for calcined powders, i.e. at 1325 °C some PbO continues to be lost from the lattice, despite the presence of excess PbO in the PBZ calcined powder, and the use of a PZ atmosphere powder. Matrix constraint and strain effects may also be a factor in suppressing the rhombohedral phase in sintered samples as the phase transformation of the orthorhombic to the rhombohedral phase is associated with a ~1 % increase in volume.

The values of sintered density as a function of PbO content are shown in Fig. 3. The density of the 3 wt % pellets was ~ 0.5 % higher than for the base composition, but density decreased for the higher PbO contents; the 10 wt % excess was over 1% lower in density compared to the base composition. The presence of a PbO - rich liquid phase usually assists densification during sintering [24-25]. However, a large amount of PbO liquid phase can produce an initial rapid densification but a lower final density as a result of void formation due to the PbO evaporation [24-25]. As a consequence the porosity of the pellet increases and this porosity is not removed by solid state sintering [17-18]. The reduction in density for the 5 and 10 wt % samples is consistent with there being an excessive amount of PbO in these samples.

The added PbO produced a slight increase in grain size in sintered samples, Fig. 4 (a-d), which is consistent with the added PbO promoting liquid phase sintering [19, 24-26]. For the base composition, the linear intercept method gave an average grain size of ~ 1 µm which increased to 1.5 ± 0.1 µm for the excess PbO samples. The fracture surfaces of the 0 and 3 wt % excess PbO samples each displayed predominantly intra-granular cleavage, whereas the 5 and 10 wt % samples showed predominantly inter-granular fracture, Fig. 4 (e-h). This indicates that the grain boundaries are weaker in the two higher excess PbO samples, consistent with residual PbO being present at the grain boundaries, causing a change in fracture mode. A weakness in the grain boundaries of other Pb-based ceramics has previously been reported when PbO is present [19-20, 24], and it is known that the morphology of the fracture surface relates to the grain boundary behavior [30]. However PbO was not detected in corresponding XRD patterns, suggesting it to be present at levels below the XRD detection limit or in poorly crystallised form after cooling from the liquid formed during sintering. The

extent to which the slightly lower density of the 5 and 10 wt % samples affected fracture morphology is uncertain.

Plots of dielectric constant and loss, Fig. 5, revealed the paraelectric transition to occur at ~ 196-197 °C for all samples, Table 1. There was however an increase in peak dielectric constant from 11500 for the 0% sample to 12700 for the 3 wt % sample, followed by reductions for the 5 and 10 wt % samples, Table 1. This trend matches that of the sintered densities, i.e. the lower density samples gave lower measured dielectric constants. No evidence of AFE-FE phase transitions were observed in any samples.

4. Conclusions

We have for the first time demonstrated the effect of excess PbO in stabilising the rhombohedral phase relative to the orthorhombic phase in Pb_{0.9}Ba_{0.1}ZrO₃ powders and ceramics. Excess PbO produced an increase in grain size in the sintered samples, from an average of ~1 µm for the unmodified composition to ~1.5 µm for the excess PbO compositions; there was also a change from intra to inter-granular fracture for compositions with > 3 wt % excess PbO. The results also indicate that ~3 wt% excess PbO produced the highest density ceramics exhibiting the maximum value of peak dielectric constant.

Acknowledgments

This work was supported by The Thailand Research Fund, Ministry of university

Affairs and Graduate School, Chiang Mai University. The authors would like to thank Prof.

Dr. Tawee Tunkasiri for his help in many facilities. Thanks are also expressed to colleagues at the University of Leeds for practical advice.

References

- G. Shirane, E. Sawaguchi, Y. Takagi, Phys. Rev. 84 (1951) 476.
- [2] R.W. Whatmore, A.M. Glazer, J. Phys. C: Solid State Phys. 12 (1979) 1505.
- [3] S. Teslic, T. Egami, Acta Crystallogr. B 54 (1998) 750.
- [4] X. Dai, J. Li, D. Viehland, Phys. Rev. B 51 (1995) 2651.
- [5] V.J. Tennery, J. Am. Ceram. Soc. 49 (1966) 483.
- [6] B.A. Scott, G. Burns, J. Am. Ceram. Soc. 55 (1972) 331.
- [7] G. Shirane, Phys. Rev. 86 (1952) 219.
- [8] G. Shirane, S. Hoshino, Acta Cryst. 7 (1954) 203.
- [9] I.H. Ismailzade, O.A. Samedov, Phys. Stat. Sol. (a) 90 (1985) 445.
- [10] Z. Ujma, J. Handerek, M. Pawelczyk, D. Dmytrow, Ferroelectrics 129 (1992) 127.
- [11] K.H. Yoon, S.C.Hwang, J. Mater. Sci. 32 (1997) 17.
- [12] B.P. Pokharel, M.K. Datta, D. Pandey, J. Mater. Sci. 34 (1999) 691.
- [13] B.P. Pokharel, D. Pandey, J. Appl. Phys. 86 (1999) 3327.
- [14] B.P. Pokharel, D. Pandey, J. Appl. Phys. 88 (2000)5364.
- [15] B.P. Pokharel, D. Pandey, J. Appl. Phys. 90 (2001)2985.
- [16] R.L. Holman, R.M. Fulrath, J. Appl. Phys. 44 (1973) 5227.
- [17] A.I. Kingon, J.B. Clark, J. Am. Ceram. Soc. 66 (1983) 253.
- [18] A.I. Kingon, J.B. Clark, J. Am. Ceram. Soc. 66 (1983) 256.
- [19] E.R. Nielsen, E. Ringgaard, M. Kosec, J. Eur. Ceram. Soc. 22 (2002) 1847.
- [20] B. Song, D. Kim, S. Shirasaki, H. Yamamura, J. Am. Ceram. Soc. 72 (1989) 833.
- [21] Y.W. Nam, K.H. Yoon, Mater. Res. Bull. 33 (1998) 331.
- [22] M. Cerqueir, R.S. Nasar, E.R. Leite, E. Longo, J.A. Varela, Ceram. Int. 26 (2000) 231.
- [23] M. Wang, M. Huang, N. Wu, Mater. Chem. Phys. 77 (2002) 103.

- [24] F. Xia, X. Yao, J. Mater. Sci. 36 (2001) 247.
- [25] L. Zhou, A. Zimmermann, Y. Zeng, F. Aldinger, J. Mater. Sci.: Mat. Elec. 15 (2004) 145.
- [26] Y. Zhang, A. Kuang, H.L. Chan, Microelectron. Eng. 66 (2003) 918.
- [27] Powder Diffraction File no.81-2042, International Centre for Diffraction Data, Newton Square, PA, 2000.
- [28] Powder Diffraction File no.76-1796, International Centre for Diffraction Data, Newton Square, PA, 2000.
- [29] Powder Diffraction File no.85-1287, International Centre for Diffraction Data, Newton Square, PA, 2000.
- [30] B. Lawn, Fracture of Brittle Solids (Cambridge University Press, Cambridge, 1993).

FIGURE CAPTIONS

Fig. 1. XRD patterns of calcined powders of PBZ made from starting powders containing different amounts of excess PbO: (+) PbZrO3 [27], (*) PbO (tetragonal phase) [28] and (x) PbO (orthorhombic phase) [29].

Fig. 2. a) Intensity of (130)/(112), (210), (230)/(212) XRD peaks as a function of PbO starting excess; b) value of intensity ratio, I_{004/240} for calcined powders and sintered pellets as a function of PbO starting excess.

Fig. 3. Variation of density of sintered pellets measured by Archimedes' method as a function of starting PbO excess.

Fig. 4. SEM micrographs of the as-sintered and fractured surfaces of sintered PBZ pellets made from starting powders with different PbO contents: (a) and (e) 0 wt%, (b) and (f) 3 wt%, (c) and (g) 5 wt%, (d) and (h) 10 wt%.

Fig. 5. Dielectric constant and dielectric loss versus temperature for PBZ ceramics made from powders with different amounts of starting excess PbO.

TABLE CAPTION

Table 1. Values of peak dielectric constant, and peak temperature (from Fig. 5)

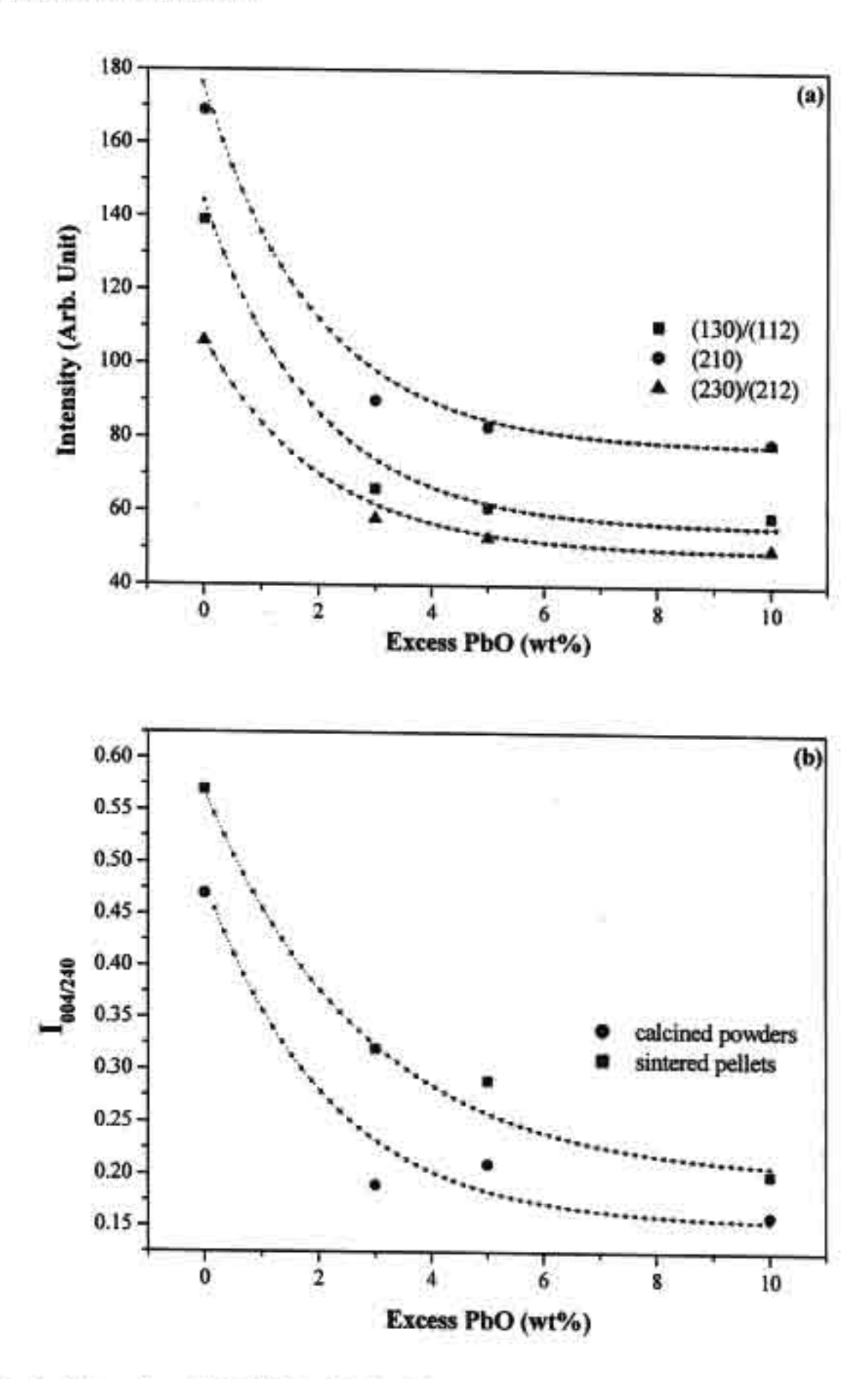


Fig. 2. a) Intensity of (130)/(112), (210), (230/212) XRD peaks as a function of PbO starting excess; b) values of intensity ratio, I_{004/240} for calcined powders and sintered pellets as a function of PbO starting excess.

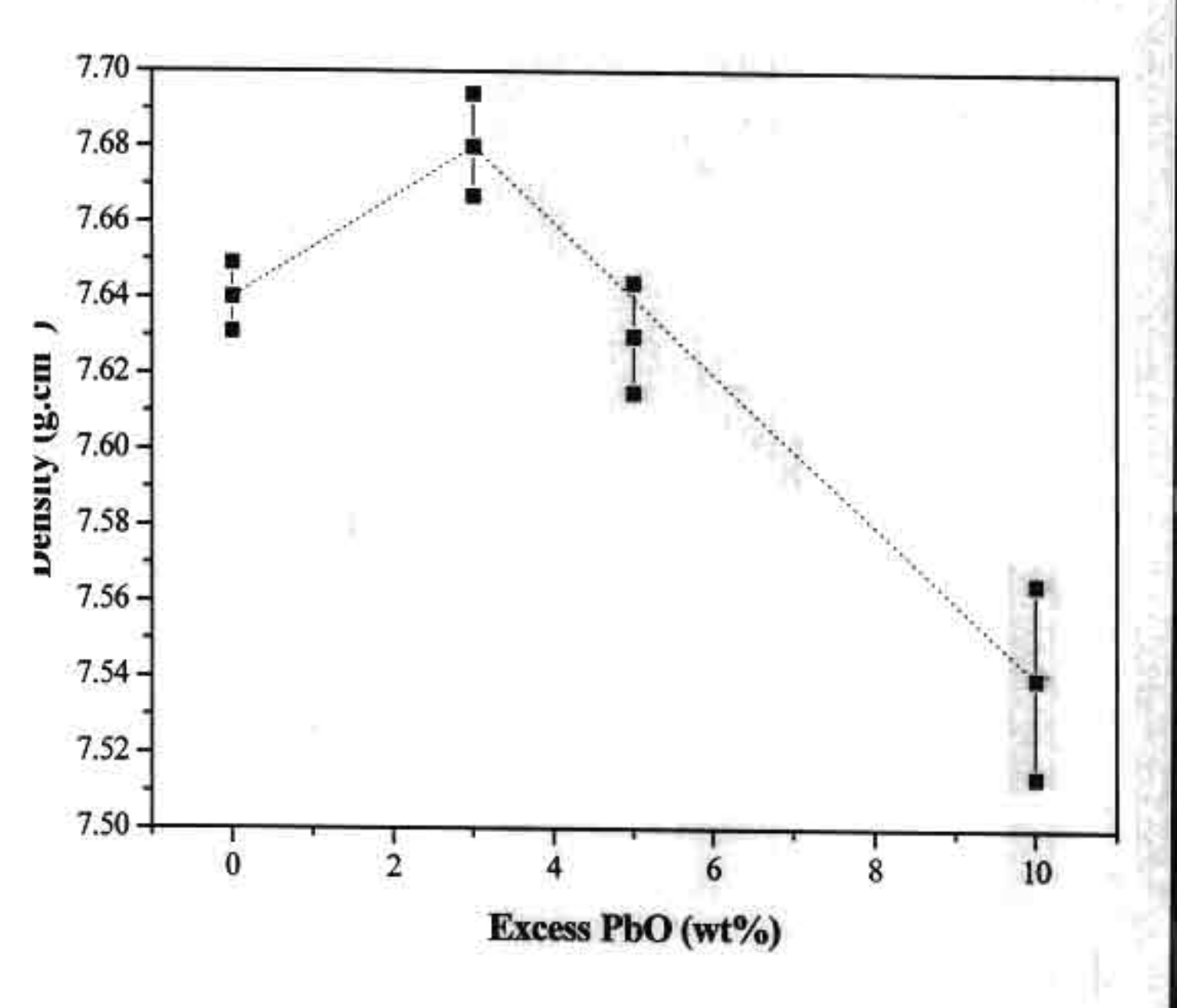


Fig. 3. Variation of density of sintered pellets measured by Archimedes' method as a function of starting PbO excess.

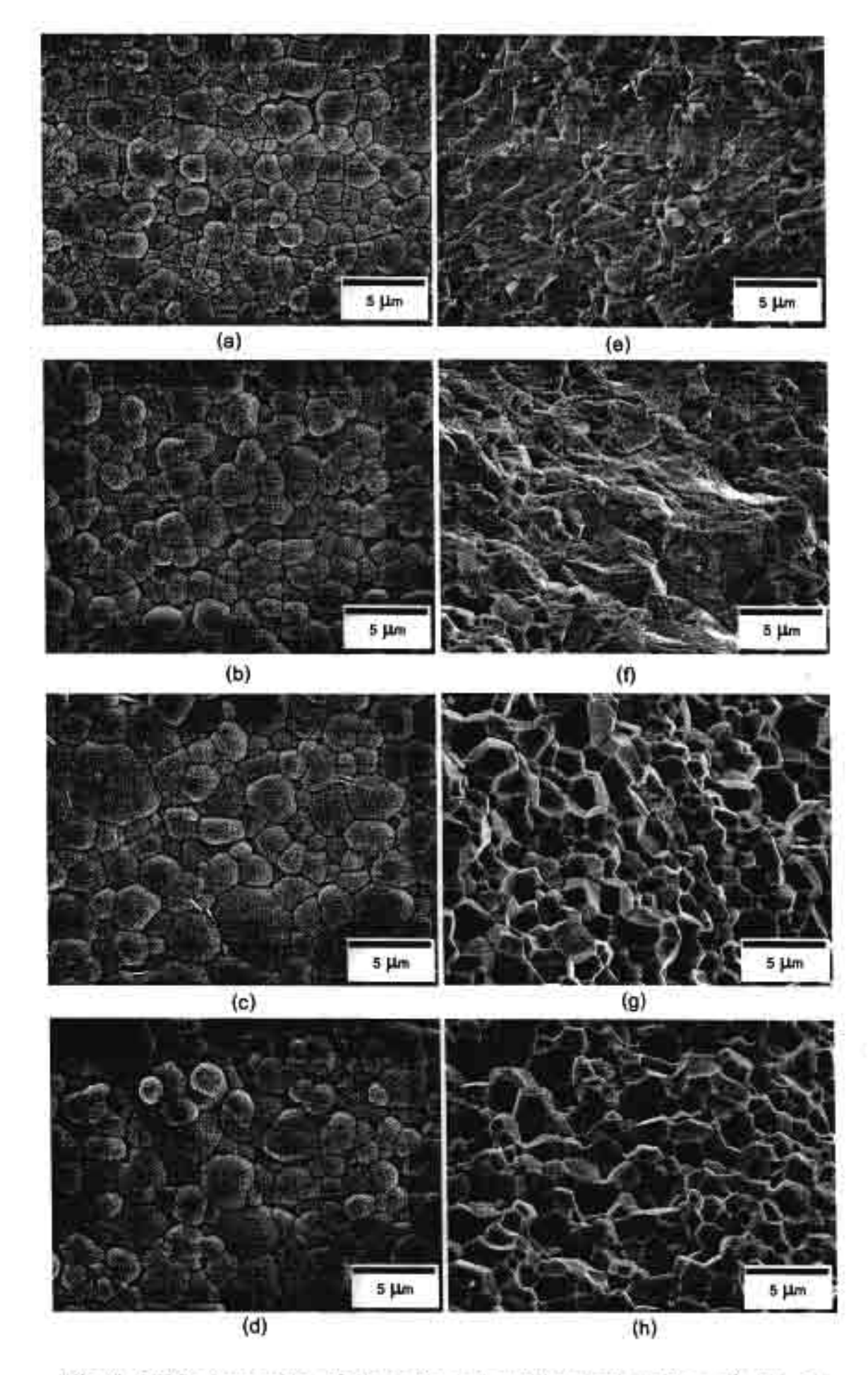


Fig. 4. SEM micrographs of the as-sintered and fractured surfaces of sintered PBZ pellets made from starting powders with different PbO contents: (a) and (e) 0 wt%, (b) and (f) 3 wt%, (c) and (g) 5 wt%, (d) and (h) 10 wt%.

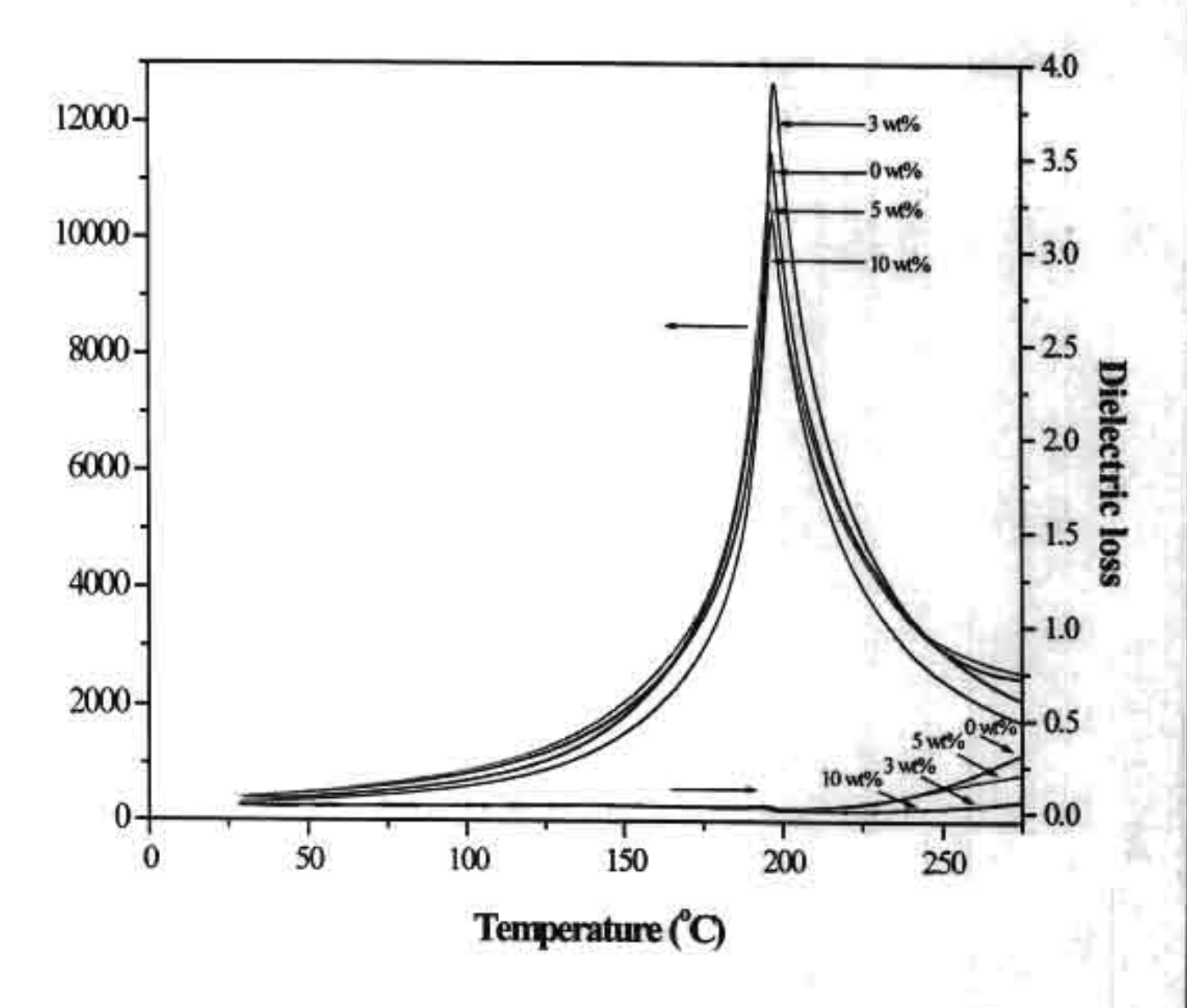


Fig. 5. Dielectric constant and dielectric loss versus temperature for PBZ ceramics made from powders with different amounts of starting excess PbO.

Table 1. Values of peak dielectric constant, and peak temperature (from Fig. 5)

Amount of PbO excess (wt%)	Maximum dielectric constant at the phase transition	Transition temperature (°C)
0	11500	197
3	12700	197
5	10600	196
10	10300	197

The Morphotropic Phase Boundary and dielectric properties of xPb(Zr_{1/2}Ti_{1/2})O₃ – (1-x)Pb(Ni_{1/3}Nb_{2/3})O₃ perovskite solid solution.

Naratip Vittayakorn, Gobwute Rujijanagul Department of Physics Faculty of Science Chiang Mai University Chiang Mai 50200 THAILAND

Xiaoli Tan, Meagen A. Marquardt, and David P. Cann. Materials Science and Engineering Department Iowa State University Ames, IA 50011 USA

Abstract

The solid solution between the normal ferroelectric $Pb(Zr_{1/2}Ti_{(/2)}O_3$ (PZT) and relaxor ferroelectric $Pb(Ni_{1/2}Nb_{2/3})O_3$ (PNN) was synthesized by the columbite method. The phase structure and dielectric properties of xPZT-(1-x)PNN where x=0.4-0.9 and the Zr/Ti composition was fixed close to the MPB were investigated. With these data, the ferroelectric phase diagram between PZT and PNN has been established. The relaxor ferroelectric nature of PNN gradually transformed towards a normal ferroelectric state towards the composition 0.7PZT-0.3PNN, in which the permittivity was characterized by a sharp peak and the disappearance of dispersive behavior. XRD analysis demonstrated the coexistence of both the rhombohedral and tetragonal phases at the composition 0.8PZT-0.2PNN; a new morphotropic phase boundary within this system. Examination of the dielectric spectra indicates that PZT-PNN exhibits an extremely high relative permittivity near the MPB composition. The permittivity shows a shoulder at the rhombohedral to tetragonal phase transition temperature, $T_{RT} = 195^{\circ}C$, and then a

maximum permittivity (36,000 at 10 kHz) at the transition temperature T $_{max}$ = 288°C at the MPB composition. The maximum transition temperature of this system was 340°C at the composition x=0.9 with the relative permittivity of 32,000 at 10 kHz.

Keywords: Morphotropic phase boundary; Lead zirconate titanate (PZT); Lead nickel niobate (PNN); Ferroelectric phase transition.

PACS number: 77.22.ch; 77.22.Gm; 77.80.Bh; 77.84.Dy

I. INTRODUCTION

The relaxor ferroelectric lead nickel niobate [Pb(Ni_{1/3}Nb_{2/3})O₃, PNN] has been studied by numerous researchers since its discovery by Smolenskii and Agranovskaya in 1958. At room temperature, single crystal PNN has the cubic prototype symmetry Pm3m with a lattice parameter (a) = 4.03Å. Nanometer-level chemical heterogeneity in the form of short range ordering of Ni²⁺ and Nb⁵⁺ on the B-site was proposed to account for the diffuse phase transition. The complex perovskite shows a broad maximum of the dielectric permittivity near -120°C with relative permittivity near 4,000 at 1 kHz.

In the last decade, normal ferroelectric lead zirconate titanate [Pb(Zr_{Fx}Ti_x)O₃, PZT] has become one of the most important commercially produced piezoelectric materials. See Excellent piezoelectric properties have been observed in compositions close to the morphotropic phase boundary (MPB Zr;Ti ~52:48). Recently, many piezoelectric ceramic materials have been developed from binary systems containing a combination of relaxor and normal ferroelectric materials which yield high dielectric permittivities (e.g. PMN-PT⁹, PZN-PT^{10,11}, PMN-PZT¹²), excellent piezoelectric coefficients (e.g. PZN-PT^{10,11}, PZN-PZT¹³, PSN-PT^{14,15}), and high pyroelectric coefficients (e.g. PNN-PT-PZ).

Fan and Kim¹³ investigated the solid solution within the PZN-PZT binary system in which the Zr/Ti composition was close to the MPB. This study indicated the composition 0.5PZN-0.5PZT showed the optimal piezoelectric properties. Moreover, these properties could be improved by thermal treatments. In 1974 Luff et al. 16 investigated solid solution in the PNN-PZ-PT ternary system and observed excellent piezoelectric properties at the composition 0.5PNN-0.35PT-0.15PZ. There have been

numerous papers published dealing with piezoelectric and processing issues within this compositional family.

16-19 These compositions have found wide applications and are now commercially available. However, there is limited information in the literature on the PNN-PZT system with Zr/Ti close to the MPB. Detailed reaction kinetics using conventional solid state processing of Pb(Ni_{1/3}Nb_{2/3})O₃-Pb(Zr_{0.48}Ti_{0.52})O₃ was recently investigated by Babushkin.

A sequence of pyrochlore phases were detected at different temperatures, but there is no information pertaining to the dielectric and ferroelectric properties.

Since PNN is a relaxor ferroelectrics with a broad dielectric peak near $T_c \approx -120^{\circ}\text{C}$ and PZT (Zr/Ti=50/50) is a normal ferroelectric with a sharp maximum permittivity at T_c $\sim 390^{\circ}\text{C}$, the curie temperature in PNN-PZT system can be engineered over a wide range of temperature by controlling the amount of PZT in the system. The aim of this work was to investigate the quasi-binary solid solution xPZT (Zr/Ti=50/50) -(I-x)PNN, with x=0.4-0.9. Figure 1 schematically shows the pseudo-ternary composition range which was studied in this work compared with other studies. Although pure PNN-PZ-PT ternary ceramics can be fabricated by conventional methods 16 , the B-site precursor method is a better method for enhancing the dielectric properties and ferroelectric properties. This process involves pre-reacting the B-site cations to form the columbite phase NiNb₂O₆ and the wolframite phase ZrTiO₄. With this method it is possible to obtain a homogeneous perovskite solid solution without the other constituent perovskite phases such as PZ, PT, PZT, PNN and the formation of the parasitic pyrochlore phases is prevented. Finally, the nature of the relaxor-normal ferroelectric phase transition was studied through a combination of dielectric measurements and x-ray diffraction.

II. Experimental

The powders of xPZT - (1-x)PNN were synthesized using the columbite precursor method. Reagent-grade oxide powders of PbO, ZrO₂, TiO₂, ZnO and Nb₂O₅, were used as raw materials. The columbite structure (ZnNb₂O₆) and wolframite structure (ZrTiO₄) were synthesized first. Stoichiometric amounts of the precursors (ZnO, Nb₂O₅) and (ZrO₂, TiO₂) were mixed and milled in isopropyl alcohol for 6 hours using a vibratory mill. The mixture was dried at 60°C for 12 hours. The precursors ZnNb₂O₆ and ZrTiO₄ were calcined at 975°C and 1400°C, respectively, for 4 hours in a closed alumina crucible. The calcined ZnNb₂O₆ and ZrTiO₄ powders were mixed with PbO in a stoichiometric ratio to form the composition xPZT - (1-x)PNN, where x = 0.4-0.9 (shown in Fig 1). In all compositions, 2 mol % excess PbO was added to compensate for lead volatilization during calcination and sintering. After re-milling and drying, the mixtures were calcined at 950°C for 4 hours in a double alumina crucible configuration with a heating rate of 10°C/min.

The calcined powders were milled for 3 hours for reduced particle size. After grinding and sieving, the calcined powder was mixed with 5 wt% poly (vinyl alcohol) binder and uniaxially pressed into a pellet. Binder burnout occurred by slowly heating to 500°C and holding for 2 hours. Sintering occurred between 1100 - 1250°C with a dwell time of 4 hours. To mitigate the effects of lead loss during sintering, the pellets were sintered in a closed alumina crucible containing PbZrO₃ powder.

The perovskite phase was examined by x-ray diffraction (XRD). Data collection was performed in the 2θ range of $20^{\circ} - 70^{\circ}$ using step scanning with a step size of 0.02° and counting time of 2s/step.

After surface grinding, the samples were electroded using sputtered gold and airdried silver paint was applied. The relative permittivity (ε_i) and dissipation factor (tan δ) were measured using an automated measurement system. This system consisted of an LCR meter (HP-4284A, Hewlett-Packard Inc.) in connection with a Delta Design 9023 temperature chamber and a sample holder (Norwegian Electroceramics) capable of high temperature measurement. The capacitance and dissipation factors of sample were measured at 100 Hz, 1 kHz, 10 kHz and 100 kHz and temperature varied between 25 – 450°C. A heating rate of 3°C/minute was used during measurements.

Samples were prepared for optical analysis by polishing with SiC paper through 1200-grit. Raman spectra were measured using a Renishaw inVia Reflex Raman microscope and 488 nm radiation from a laser excitation source. The laser had an output power of 25 mW and a focused spot size of 200-300 µm through a 5x microscope objective. Raman spectra were measured using a static acquisition centered at 520 cm⁻¹ and 15 accumulations with 2-second exposure times.

III. Results and Discussion

A. Crystal structure and phase transition studies

Perovskite phase formation, crystal structure and lattice parameter was determined by XRD at room temperature as a function of x. Figure 2 shows XRD patterns of ceramics in the xPZT - (1-x)PNN system with a well crystallized perovskite structure for all compositions. The pyrochlore phase was not observed in this system at all. The crystal symmetry for pure PNN at room temperature is cubic Pm3m with a

lattice parameter a=4.031 Å. Below $T_{max}\approx -120^{\circ}C_s$ the symmetry changes to rhombohedral. The crystal structure of Pb($Zr_{1/2}Ti_{1/2}$)O₃ at room temperature is tetragonal. Therefore, with increasing x the crystal symmetry should change due to the effects of the increased PZT fraction and the increase in T_C . Figure 3 shows XRD peak profiles of the (200) and (220) peaks at x=0.4, 0.5, and 0.6. The XRD data shows that the splitting of (200) peak is not observed. At the x=0.4 composition, only a single (220) peak is seen, indicating that the major phase in this composition had cubic symmetry. However splitting was very clearly observed for the (220) peak in compositions x=0.5 and 0.6, indicating that the crystal transformed into rhombohedral symmetry (pseudo-cubic). With a further increase in PZT content to x>0.6, the (111) and (200) diffraction peaks begin to split as shown in Fig 4. Splitting of the (200) peak becomes more pronounced as x approaches 0.9 indicating a stabilization of the tetragonal phase at high PZT concentrations.

At the x = 0.8 composition, the unambiguous splitting of (111) peak indicates the co-existence of the rhombohedral and tetragonal phase. Thus there is a transformation from the rhombohedral phase to the tetragonal phase across the compositional range x = 0.7-0.9. The x = 0.7 composition is within the rhombohedral-rich side of the MPB and the composition x = 0.9 is on the tetragonal-rich side of the MPB. It is important to note that recent results have uncovered the existence of a low-symmetry (monoclinic) phase within the MPB region of PZT²⁴, PMN-PT ²⁵ and the orthorhombic phase of PZN-PT²⁶. Given the similarities of PNN-PZT to the PMN-PT system, it is possible that a low symmetry monoclinic or orthorhombic phase may be stabilized within the MPB regions of xPZT – (1-x)PNN; x = 0.7-0.9.

B. Dielectric properties

The characteristic temperature and frequency dependence of the relative permittivity for xPZT-(I-x)PNN, x=0.4-0.9 is shown in Figure 5. A clear transition in T_{max} (defined as the temperature at which ε_r is maximum at 10 kHz) is observed with T_{max} increasing with x. At compositions x=0.4, 0.5 and 0.6, the sample displays a pronounced relaxor ferroelectric behavior, characterized by diffuse permittivity peaks and a shift of the maximum permittivity to higher temperatures with increasing frequency. An increase in the magnitude of the maximum permittivity is also observed over this region. The nature of the homogeneously polarized states is believed to be controlled by the concentration of PZT.

A smooth transition from relaxor to normal ferroelectric behavior is observed with increasing mole percent of PZT from x = 0.7 to 0.9. This transition is characterized by the enhancement of the first-order nature of the phase transformation and the diminishment of the relaxor behavior (i.e. the permittivity dispersion) over the broad temperature range in the vicinity of T_{max} . From these data, the relaxor-normal transformation is very clearly observed with increased PZT concentration above x=0.7. Furthermore, the relative permittivity and T_{max} increased with increased mole percent of PZT considerably up to a maximum permittivity at x=0.8. The sharp permittivity peak exhibits a maximum value of 36,000 at 10 kHz for this composition. Figure 6 shows a comparison of the permittivity as a function of temperature for the compositions x=0.5, 0.7, and 0.8 taken over the measurement frequencies of 100 Hz - 100 kHz.

For x = 0.5, T_{max} increases from 125.6°C at 100 Hz to 130.8 °C at 100 kHz ($\Delta T = 5.2$ °C). The relative permittivity at room temperature was 2,830 at 100 Hz and

increased to 24,200 at 1 kHz at T_{max} , and the maximum value of the relative permittivity decreased with increasing frequency. The dielectric dispersion below T_{max} indicates typical relaxor ferroelectric behavior arising from the responses of polar micro-domains within the spectrum of the relaxation time. For x = 0.7 and 0.8 compositions, it is evident that two phase transitions are observed. Over the temperature range 190 to 200°C, a rhombohedral to tetragonal phase transition is observed for both compositions (indicated in the figure by $T_{Rbo-Tevra}$). Another transition between the ferroelectric tetragonal to paraelectric cubic phase occurs in the temperature ranges 225°C and 277°C for x = 0.7 and x = 0.8, respectively. Although the transition from ferroelectric rhombohedral to tetragonal phase is obscured in the composition x = 0.7 it is more clearly evident in the composition x = 0.8. Similar phenomena has been observed in single crystal PZN-PT¹¹, PIN-PT²⁷, and PMN-PT⁹.

In addition, the transformation from the relaxor ferroelectric state to the normal ferroelectric state can be observed in the composition x = 0.7-0.9 as shown in Figs. 5, 6b, 6c. The permittivity sharply increased near the temperature indicated as $T_{\text{start NR}}$ in Fig. 6b and 6c. The subscript "start NR" denotes the initial transition from a normal ferroelectric state to a pure relaxor ferroelectric state. Relaxor behavior was observed at temperatures above $T_{\text{flaish NR}}$. The subscript "finish NR" denotes the completion of the transformation. For x = 0.7 at temperatures below 212°C, the relative permittivity did not show any significant dispersion until 218°C. Above this temperature, the relative permittivity shows a strong frequency dependence. This indicates that at 212°C, 0.7PZT-0.3PNN started to transform from a normal ferroelectric state to a relaxor ferroelectric state; finishing the transformation at 218°C. The differential between T_{start}

 $_{NR}$ and $T_{finish\ NR}$ was approximately 6°C, 5°C and 4°C for x = 0.7, 0.8, 0.9 respectively. This behavior can be explained by decreasing relaxor stability with increasing x.

At the composition x = 0.9, a broad permittivity was observed with a slight frequency dispersion close to T_{max} . A first-order transition response was observed at temperatures slightly below T_{max} . This phenomenon indicates that the polar moments are static, since the polar moments are relative large. The crystal structure and dielectric properties for all compositions are listed in Table 1.

The maximum permittivity $\varepsilon_{r,max}$ and T_{max} as a function of the mole fraction of PZT (x) are represented in Fig. 7. There is a good linear relationship between T_{max} and x, indicating that this system is a well behaved complete solid solution. The T_{max} of the constituent compounds PNN and PZT are -120°C and 390°C, respectively, which can be used to calculate an empirical estimate of T_{max} via the equation:

$$T_{\text{max}} = x(390^{\circ}C) + (1-x)(-120^{\circ}C)$$
 (1)

The variation of the measured T_{max} , the calculated T_{max} , and the measured $\varepsilon_{r,max}$ as a function of composition x is shown in Fig. 7. The highest $\varepsilon_{r,max}$ of 36,000 at 277°C at 10 kHz was observed for the composition at the MPB 0.8PZT-0.2PNN. It is evident from the data that Eq. (1) gives a reasonable approximation of the transition temperature T_{max} . This result suggests that the transition temperature of xPZT-(1-x)PNN system can be varied over a wide range from -120 to 390°C by controlling the amount of PZT in the system.

It is well known that the permittivity of a first-order normal ferroelectric can be described by the Curie-Weiss law:

$$\frac{1}{\varepsilon} = \frac{T - \theta}{C} \tag{2}$$

where θ is the Curie-Weiss temperature and C is Curie constant. A second order relaxor ferroelectric can be described by a simple quadratic law. This arises from the fact that the total number of relaxors contributing to the permittivity response in the vicinity of the permittivity peak is temperature dependent, and the temperature distribution of this number is given by a Gaussian function about a mean value T_0 with a standard deviation δ . The relative permittivity can be derived via the following expression: 28,29

$$\frac{\varepsilon_n'}{\varepsilon'(f,T)} = 1 + \frac{(T - T_n(f))^r}{2\delta_r^2} \quad (1 \le \gamma \le 2)$$
(3)

where ε_m' is the maximum value of the permittivity at $T = T_m(f)$. The value of γ is the expression of the degree of dielectric relaxation in the relaxor ferroelectric material. When $\gamma = 1$ Eq. (3) expresses Curie-Weiss behavior, while for $\gamma = 2$ this equation is identical to the quadratic relationship. Many relaxor ferroelectric materials can be fit to Eq. (3) with $\gamma = 2$ at temperatures above T_{max} . The parameter δ_{γ} can be used to measure the degree of diffuseness of the phase transition in mixed relaxor-normal ferroelectric materials. The values γ and δ_{γ} are both material constants depending on the composition and structure of the material. The δ_{γ} value can be determined from the slope of $\varepsilon_m'/\varepsilon'$ versus $(T-T_m)^2$, which should be linear.

The δ_{γ} values of compositions in the xPZT-(1-x)PNN system are represented in Fig 8. Both the diffuseness parameter δ_{γ} and γ decreased with an increase in the mole fraction of PZT. As illustrated in Fig. 9, a near linear relationship was observed over the wide compositional range which is consistent with a perfect solid solution. The diffuseness of the phase transition in the x = 0.4 composition can be attributed to the relaxor nature of PNN. As the PZT content increased, the relaxor characteristic of xPZT-(I-x)PNN was observed to decrease. This is because the substitution of $(Zr_{1/2}Ti_{1/2})^{4+}$ for the B-site complex ions $(Ni_{1/3}Nb_{2/2})^{4+}$ increases the size of the local polar domains by strengthening the off-center displacement and enhancing the interactions between micropolar domains. As was observed in PMN-PT crystals³⁰, this leads to the formation of macro-polar domains which break the symmetry of the pseudo-cubic state.

C. Raman spectroscopy of Pb(Zr10Ti10)O3-Pb(Ni10Nb20)O3

Figure 10 shows the Raman spectra of ceramic xPZT-(I-x)PNN with x=0.4 to 0.9. The individual spectral data was analyzed using Bruker Optics OPUS software: A multi-peak pattern was fit to the data using Lorentz-Gauss peak shape parameters and Levenberg-Marquardt refinement techniques. The resulting peak locations for each xPZT-(1-x)PNN sample is shown in Figure 11. Each peak represents a Raman active vibration mode frequency for the given composition. Peak location and intensity will vary depending on the type of bonds present in the material. There is a distinct difference in pattern when going from x=0.4-0.5. The disappearance of modes at 440 and 560 cm⁻¹ and the appearance of modes at 675 and 890 cm⁻¹ are indicative of a change in phase. The same is indicated for x=0.7-0.8, where a weak mode at 350 cm⁻¹ first appears at x=0.7 and gains intensity for x=0.8-0.9. There is yet another change in mode pattern when

going from x = 0.8-0.9, where modes appear at 250, 670, and 834 cm⁻¹. These modes represent the splitting of a single mode for x = 0.8.

D. Phase diagram of Pb(Zr12Ti12)O3-Pb(Ni13Nb23)O3

Based on the results of x-ray diffraction, dielectric spectroscopy, and Raman spectroscopy, the phase diagram for the xPZT-(1-x)PNN binary system have been established, shown in Fig. 12. The transition temperature increases approximately linearly with x, from $T_{max} = 75^{\circ}$ C for x = 0.4 to 340° C for x = 0.9. The phase diagram consists of four distinct crystallographic phases in this system; high temperature paraelectric cubic (Pm3m), pseudo-cubic relaxor, rhombohedral relaxor (R3m), and normal ferroelectric tetragonal (P4mm). At low concentrations of PZT $x \le 0.4$ the symmetry of can be defined as pseudo-cubic. The pseudo-cubic symmetry transforms into rhombohedral at the composition near x = 0.5. The ferroelectric rhomohedral and tetragonal phases are separated by a morphotropic phase boundary (MPB) region which is located near the composition x = 0.8 below 277° C. Within this region, both the rhomohedral and tetragonal phases coexist.

IV. Conclusions

In this work the ferroelectric properties of the solid solution between relaxor ferroelectric PNN and normal ferroelectric PZT(50/50) have been investigated. The crystal structure data obtained from XRD indicates that the solid solution x PZT-(I-x)PNN, where x = 0.4-0.9, successively transforms from pseudo-cubic to rhombohedral

to tetragonal symmetry with an increase in PZT concentration. The new MPB in this binary system is located near x = 0.8, separating the rhombohedral and tetragonal phases. At the MPB composition, the permittivity exhibited a shoulder at $T_{RT} = 195$ °C indicating a rhombohedral to tetragonal phase transformation with a maximum permittivity of 36,000 at 10 kHz at T max = 288°C. Moreover a transition from relaxor to normal ferroelectric behavior is clearly observed above a PZT concentration x = 0.7. Furthermore, this transition between relaxor to normal ferroelectricity was typified by a quasi-linear relationship between the diffuseness parameter δ_r and PZT mole fraction x.

Acknowledgements

The authors are grateful to the Thailand Research Fund (TRF), Graduate School of Chiang Mai University, and the Ministry of University Affairs for financial support.

Table I. Ferroelectric properties of x PZT-(1-x) PNN ceramics

Composition x	Crystal structure	T _m (°C) at 10 kHz	Relative permittivity at 25°C	Relative permittivity at T _{max}	tan δ at 25°C	tan δat T _m	δη
x = 0.4	С	75.4	7500	17500	0.062	0.036	29.5
x = 0.5	R	128.9	2500	22000	0.042	0.024	24.4
x = 0.6	R	169.7	1600	27000	0.042	0.018	22.4
x = 0.7	R-rich	225.5	1060	31200	0.029	0.025	14.0
x = 0.8	R+T	277.4	835	36000	0.011	0.047	10.2
x = 0.9	T-rich	326.7	950	32000	0.005	0.182	8.6

C = cubic, R = rhombohedral, T = tetragonal

Reference

- G. A. Smolenskii and A. L. Agranovskaya, Sov. Phys.-Tech. Phys., 1380 (1958).
- V. A. Bokov and I. E. Myl'nikova, Sov. Phys.-Solid state 3, 613 (1961).
- 3 C. A. Randall and A. S. Bhalla, Jpn.J.Appl.Phys. 29, 327 (1990).
- 4 V. A. Bokov and I. E. Mylnikova, Sov. Phys-Solid State 2, 2428 (1960).
- 5 K. Uchino, Ferroelectric Devices (Marcel Dekker, Inc., New York, 2000).
- A. J. Moulson and J. M. Herbert, Electroceramics Materials, Properties: Applications (Chapman and Hall, New York, 1990).
- 7 K. Uchino, Solid State Ionics 108, 43 (1998).
- 8 S.-E. Park and T. R. Shrout, IEEE Tr. UFFC. 44, 1140 (1997).
- T.R.Shrout, Z.P.Chang, N.Kim, and S.Markgraf, Ferroelectr. Lett. Sect. 12, 63 (1990).
- 10 J. Kuwata, K. Uchino, and S. Nomura, ferroelectrics 37, 579 (1981).
- M. L. Mulvihill, L. E. Cross, W. Cao, and K. Uchino, J.Am. Ceram. Soc. 80, 1462 (1997).
- H. Ouchi, K.Nagano, and S.Hayakawa, J.Am. Ceram. Soc. 48, T26-T31 (1965).
- 13 H. Fan and H.-E. Kim, J.Mater.Res. 17, 180 (2002).
- 14 Y.Yamashita, Jpn.J.Appl.Phys. 33, 4652 (1994).
- 15 V.J.Tennery, K.W.Hang, and R.E.Novak, J.Am.Ceram.Soc. 51, 671-674 (1968).
- 16 D. Luff., R. Lane, K.R. Brown, and H. J. Marshallsay, Trans. J.Br. Ceramic Soc. 73, 251 (1974).
- 17 B. EA, S. PL, S. IA, and I. VA., Bull. Acad. Sci. USSR Phys. Ser. 29, 1877 (1965).
- 18 G. Robert, M. Demartin, and D. Damjanovic, J.Am. Ceram. Soc. 81, 749 (1998).
- E. F. Alberta and A. S. Bhalla, International journal of inorganic materials 3, 987 (2001).
- O. Babushkin, T. Lindback, J. C. Luc, and J. Y. M. Leblais, J. Eur. Ceram. Soc. 18, 737 (1998).
- 21 G. Robert, M. D. Maeder, D. Damjanovic, and N. Setter, J.Am. Ceram. Soc. 84, 2869 (2001).
- 22 Z. Li and X. Yao, J.Mater.Sci.Lett. 20, 273 (2001).
- 23 M.-S. Yoon and H. M. jang, J.Appl.Phys. 77, 3991 (1995).
- 24 B. Noheda, D. E. Cox, G. Shirane, J. A. Gonzalo, L. E. Cross, and S.-E. Park, Appl. Phys. Lett. 74, 2059 (1999).
- 25 Z.-G. Ye, B. Noheda, M. Dong, D. Cox, and G. Shirane, Phys. Rev. B 64, 184114 (2001).
- D. La-Orauttapong, B. Noheda, Z.-G. Ye, P. M. Gehring, J. Toulouse, D. E. Cox, and G. Shirane, Phys. Rev. B 65, 144101 (2002).
- 27 Y. Guo, H. Luo, and T. He, Mat. Res. Bull. 38, 85 (2003).
- 28 H. T. Martirena and J.C.Burfoot, Ferroelectrics 7, 151 (1974).
- 29 K.Uchino and S.Nomura, Ferroelectr. Lett. Sect. 44, 55 (1982).
- 30 Z.-G. Ye and M.Dong, J.Appl.Phys. 87 (2000).

- Figure 1. Compositions studied in the Pb(Ni_{1/3}Nb_{2/3})O₃-PbZrO₃-PbTiO₃ ternary system
- Figure 2. XRD patterns at room temperature for xPZT (1-x)PNN ceramics.
- Figure 3. XRD patterns of the (200) and (220) peaks of xPZT (1-x)PNN ceramics, x = 0.4-0.6.
- Figure 4. XRD patterns of the (111) and (200) peaks of xPZT (1-x)PNN ceramics, x = 0.7-0.9.
- Figure 5. Temperature dependence of the relative permittivity ε_r for xPZT (1-x)PNN ceramics, x = 0.4-0.9.
- Figure 6. Temperature dependence of the relative permittivity ε_r for xPZT (1-x)PNN ceramics, A: x = 0.5, B: x = 0.7 and C: x = 0.8.
- Figure 7, T_{max}, calculated T_{max} and maximum ε_r as a function of composition x at 10 kHz
- Figure 8. Log $_{10}$ [$(\varepsilon_m/\varepsilon)$ -1] versus Log $_{10}(T-T_{max})$ for xPZT (1-x)PNN ceramics, x = 0.4-0.9.
- Figure 9 Parameter γ and degree of diffuseness (δ_{γ}) versus x for xPZT (1-x)PNN, ceramics, x = 0.4-0.9.
- Figure 10 Raman spectra of ceramic xPZT-(1-x)PNN with x = 0.4 to 0.9.
- Figure 11. Wavenumber as a function of composition x for ceramic xPZT-(I-x)PNN with = 0.4 to 0.9
- Figure 12. Phase diagram of xPZT (1-x)PNN, x = 0.4-0.9 quasi-binary system.

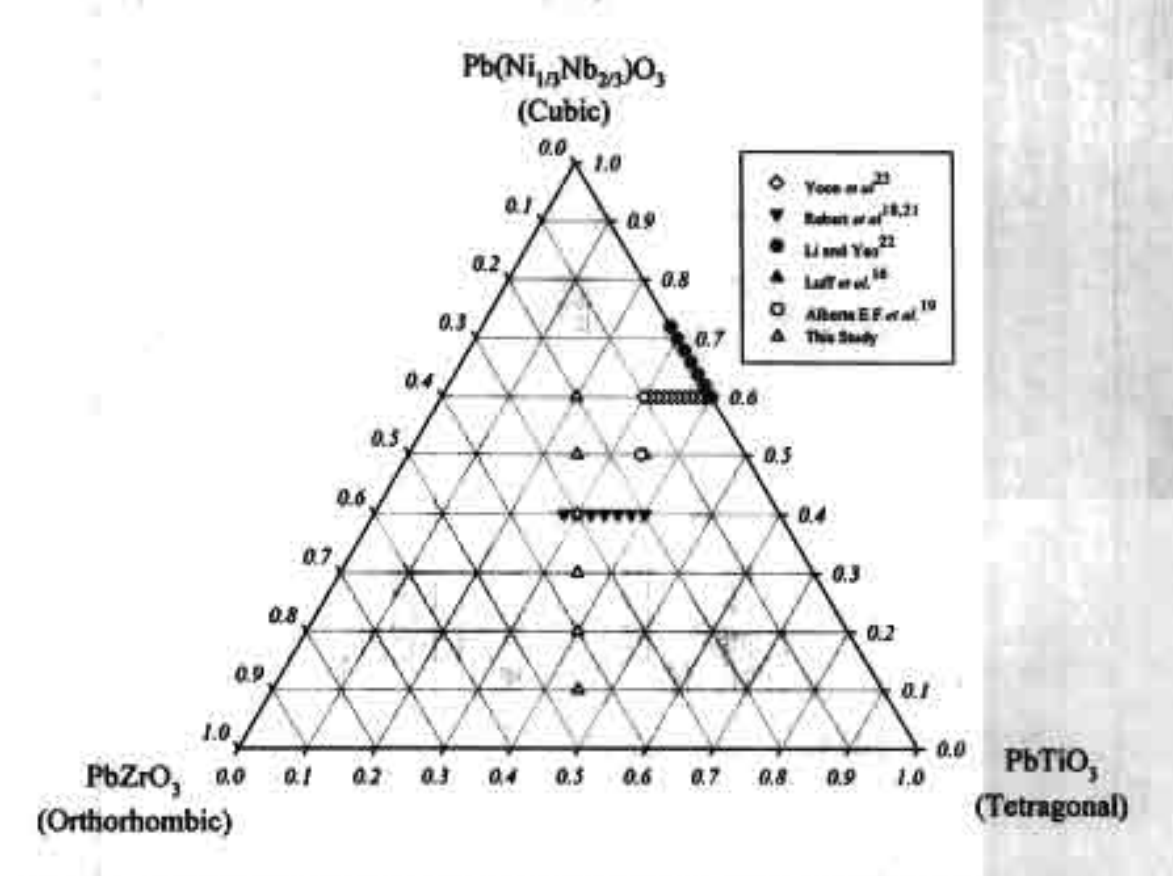


Figure 1. Compositions studied in the Pb(Ni_{1/3}Nb_{2/3})O₃-PbZrO₃-PbTiO₃ ternary system

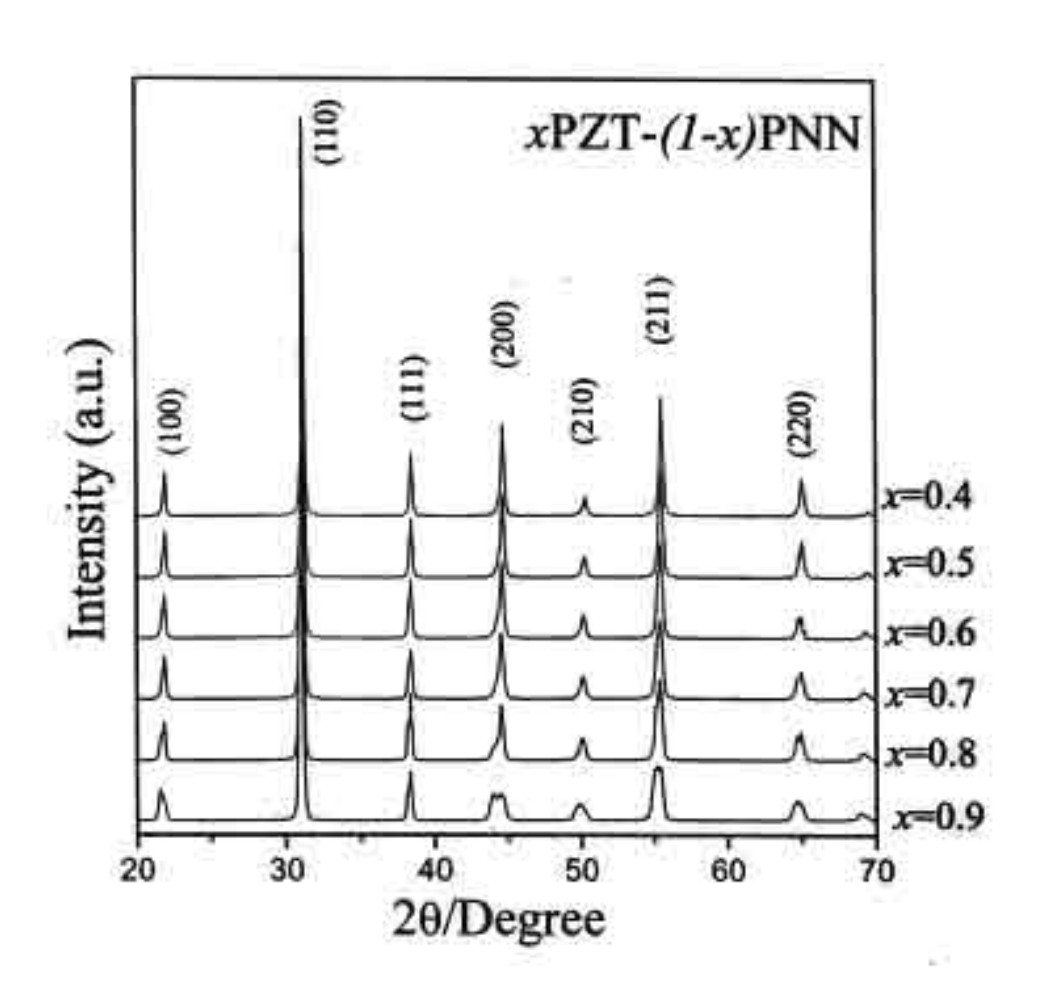


Figure 2. X-ray diffraction patterns at room temperature for xPZT - (1-x)PNN ceramics.

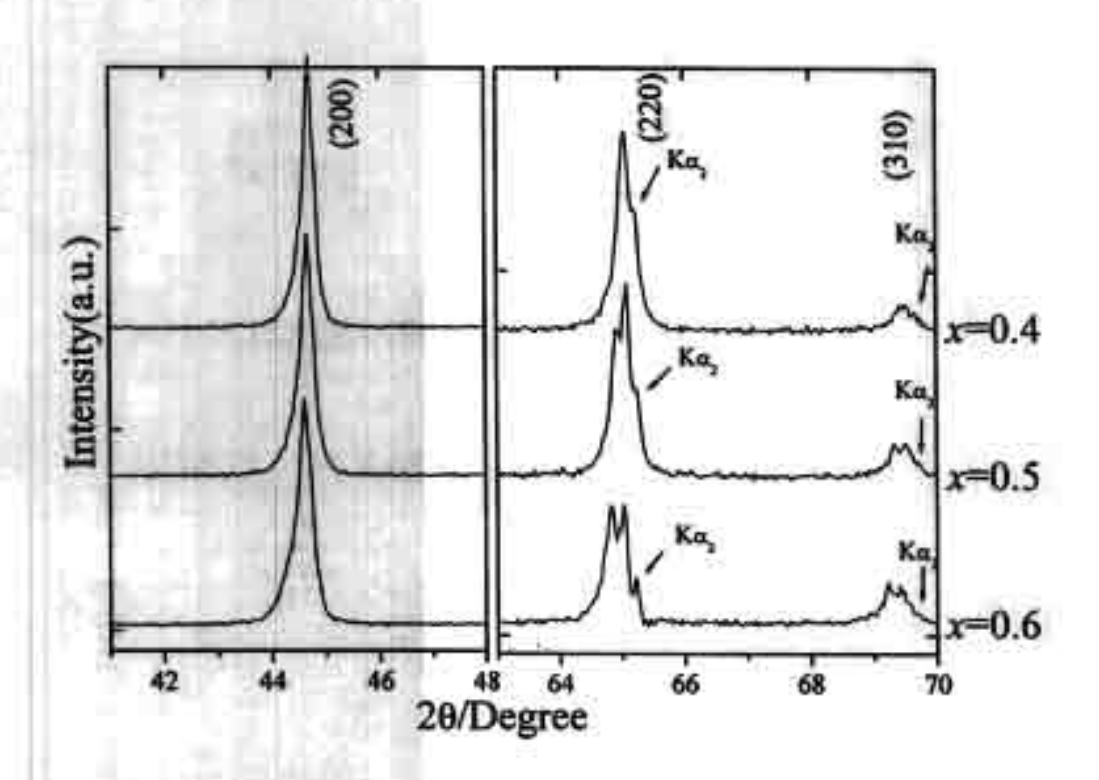


Figure 3. X-ray pattern of the (200) and (220) peak of xPZT -(1-x)PNN ,x = 0.4-0.6 ceramics.

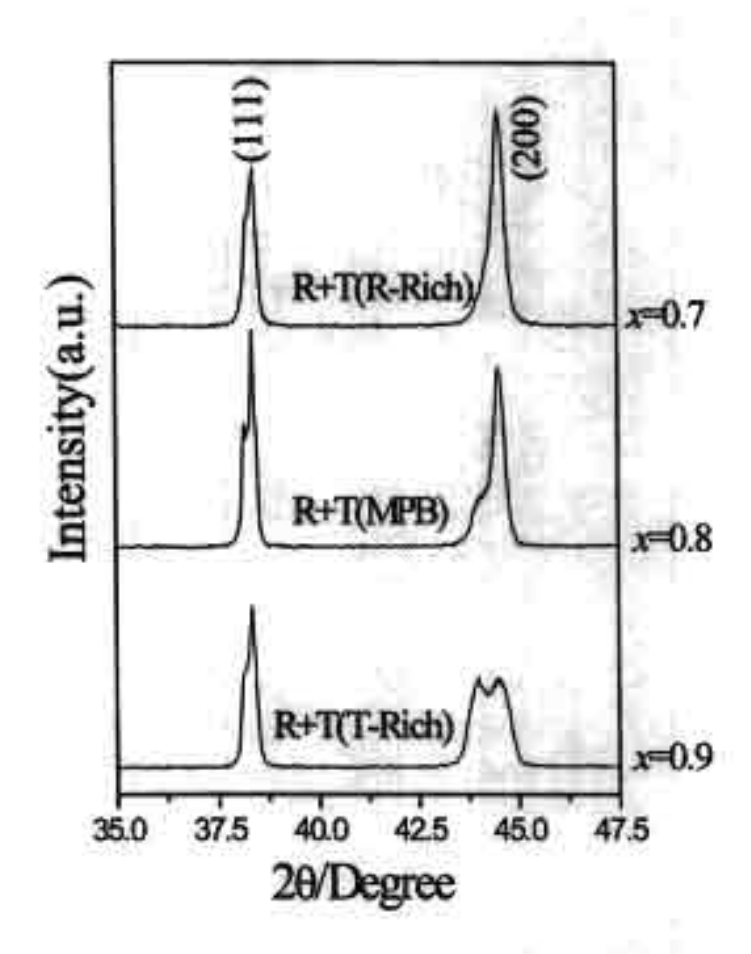


Figure 4. X-ray pattern of the (111) and (200) peak of xPZT - (1-x)PNN, x = 0.6-0.9 ceramics.

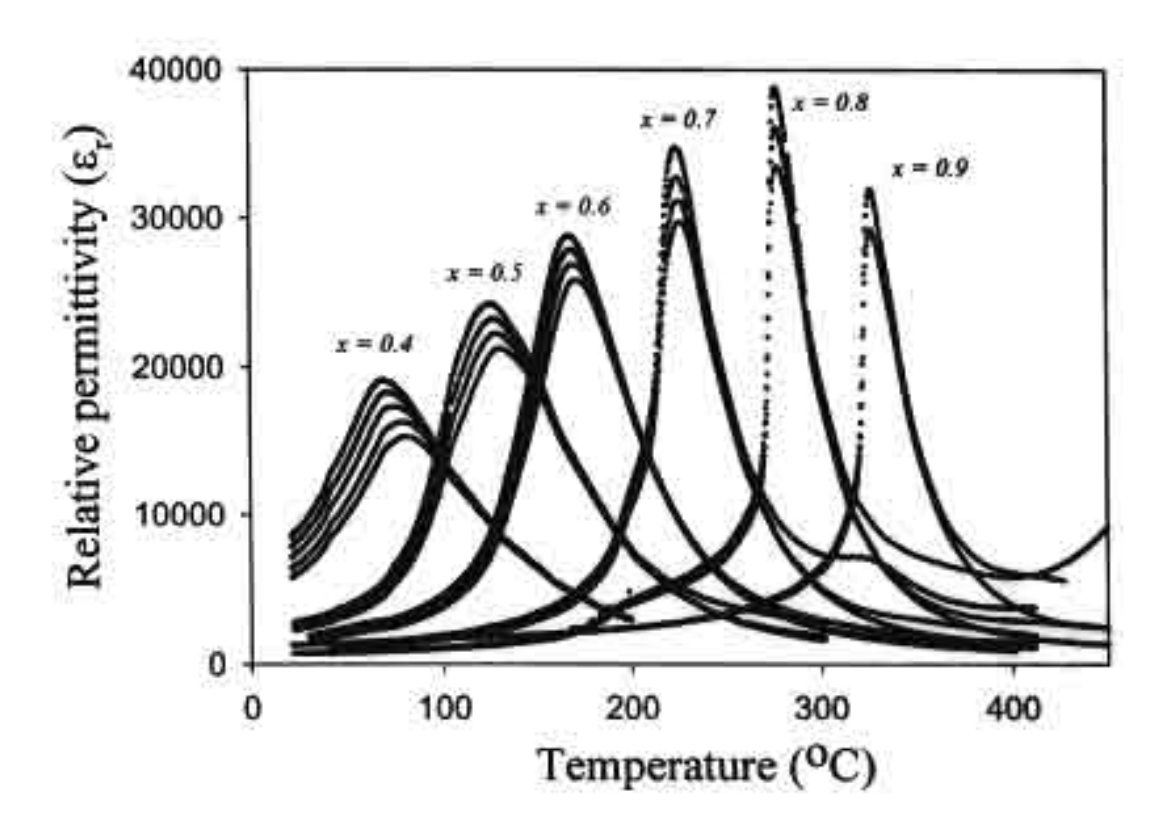


Figure 5. Temperature dependence of relative permittivity ε_r for xPZT – (1-x)PNN, x = 0.4-0.9 ceramics.